Scientific Paper / Artículo Científico

UNIVERSIDAD POLITÉCNICA SALESIANA ECUADOR
INGENIUS
Revista de Ciencia y Tecnología
https://doi.org/10.17163/ings.n34.2025.08
pISSN: 1390-650X / eISSN: 1390-860X

Modeling of an Electromagnetic Cannon using ATP-EMTP and ATPDraw

Modelación de un Cañón Electromagnético utilizando ATP-EMTP y ATPDraw

José Manuel Aller[1,*], Juan José Cordero Cantos[1], Pedro José León Rojas[1], Johnny Rengifo[2]

Received: 02-04-2025, Received after review: 27-05-2025, Accepted: 29-05-2025, Published: 01-07-2025

Abstract

This study presents a computational model of an electromagnetic cannon developed using the ATP-EMTP simulation tool and its graphical interface, ATPDraw. The system features a cylindrical metallic armature that traverses multiple stages of circular coils. Employing the Voltage Behind Reactance (VBR) methodology, each coil is modeled as a dynamic equivalent circuit comprising a resistance, an inductance, and an electromotive force source. The model parameters are dynamically updated at each simulation time step based on the armature's motion. The coils are energized by pre-charged capacitors and connected through thyristors, which are triggered at specific positions of the moving armature. The model's validity is corroborated by experimental data reported in the literature, confirming the accuracy and robustness of the proposed approach. In addition to supporting the design of electromagnetic cannons, this work provides a methodological foundation for future research and practical applications in this domain.

Keywords: Electromagnetic cannon, Circular coils, Armature, Eletromagnetic Transient Program, ATP-Draw

Resumen

Este trabajo presenta un modelo de cañón electromagnético desarrollado mediante la herramienta ATP-EMTP y su entorno gráfico ATPDraw. El diseño incluye varias etapas de bobinas circulares a través de las cuales se desplaza una armadura metálica cilíndrica. Utilizando la técnica VBR, cada bobina se convierte en un equivalente dinámico, conformado por una resistencia, una inductancia y una fuente de fuerza electromotriz. Estos parámetros se determinan instantáneamente según la dinámica del sistema mecánico. Las bobinas se energizan mediante condensadores inicialmente cargados y se conectan a ellas mediante tiristores, que se disparan en momentos específicos, determinados por la posición de la pieza metálica móvil denominada armadura. La validez del modelo se verifica mediante resultados experimentales reportados en la literatura, asegurando la precisión y efectividad del enfoque propuesto. Este estudio, además de contribuir al diseño de cañones electromagnéticos, también establece una metodología de análisis para futuras investigaciones y aplicaciones en este campo.

Palabras clave: cañón electromagnético, bobinas circulares, armadura, electromagnetic transient program, ATPDraw

[1,*]Carrera de Electricidad. Universidad Politécnica Salesiana, Ecuador
Corresponding author ✉: jaller@ups.edu.ec.

[2]Departamento de Ingeniería Eléctrica, Universidad Técnica Federico Santa María, Santiago, Chile

Suggested citation: J. M. Aller, J. J. Cordero Cantos, P. J. León Rojas y J. Renjifo, "Modeling of an Electromagnetic Cannon using ATP-EMTP and ATPDraw," *Ingenius, Revista de Ciencia y Tecnología*, N.° 34, pp. 103-115, 2025, DOI: https://doi.org/10.17163/ings.n34.2025.08.

1. Introduction

The electromagnetic cannon is a device that harnesses the magnetic field generated within a solenoid, energized by an injected electric current, to accelerate metallic moving components to high velocities. This form of propulsion offers an alternative to traditional systems that rely on chemical fuels or explosives. By employing multiple stages arranged in sequence, electromagnetic cannons enable the achievement of high speeds and significant acceleration [1].

The development of electromagnetic cannons dates back to Fauchon-Villeplee's research in 1918 [2], in which he proposed the use of electrical energy for projectile acceleration. However, the technological constraints of the time, combined with the lack of adequate energy sources and materials, impeded practical implementation. Several decades later, the United States Navy revived the concept, fostering its development for military applications. Since then, advances in power electronics, novel material technologies, and sophisticated control systems have made the practical implementation of electromagnetic cannons increasingly feasible. Nonetheless, significant challenges remain, particularly in scaling the technology, enhancing its efficiency and effectiveness, and reducing associated costs.

Interest in electromagnetic cannons extends beyond military applications. Recent studies have explored their role in the propulsion of artificial satellites, offering an efficient and cost-effective alternative for launching nano-satellites [3]. In this context, Schroeder [4] introduced a model centered on space propulsion, emphasizing its potential to enhance access to space through electromagnetic launch systems.

In recent years, significant advancements have been achieved in electromagnetic cannon technology, particularly with the development of multistage synchronous induction coil systems [5–7], which enhance operational efficiency by enabling contactless projectile propulsion. The effectiveness of this approach relies on precise synchronization between the coil power supply and the projectile's motion. However, achieving such exact synchronization continues to pose a significant technical challenge.

The electromagnetic cannon model presented in this work introduces an analytical approach that integrates an electrical circuit whose parameters are dependent on the dynamics of the electromechanical system. To this end, the Voltage Behind Reactance (VBR) representation [8,9] of the governing differential equations is employed. This method derives a dynamic Thèvenin equivalent based on the system's motion-dependent equations, enabling accurate modeling of its behavior.

The model proposed in this work was implemented using the ATP-EMTP simulation tool and its graphical interface, ATPDraw. The system solves the governing differential equations through programming in MODELS modules, which calculate the parameters of the equivalent VBR circuit. These parameters are interconnected with resistances, inductances, and controlled voltage sources via signal control modules known as TACS (Transient Analysis of Control Systems) [10].

The electromagnetic behavior of the coil-armature interaction is characterized using the filament method [11], which enables the calculation of the self and mutual inductances of the coil and armature for any relative position between them. Numerical differentiation is applied to determine the positional variation of these inductances, which are essential for computing both the electric force and the electromotive force acting on the coil. Although the detailed derivation lies beyond the scope of this work, the resulting inductance values and their spatial derivatives are incorporated into the ATP-EMTP model through MODELS programming.

2. Materials and Methods

2.1. Problem Statement

The electromagnetic cannon converts electrical energy into mechanical energy through forces generated by the interaction between the magnetic field produced by the coil current and the field induced in the armature. This interaction results in the acceleration of the armature as it moves through the coil. The effectiveness of the energy conversion depends on the current, dimensions, and geometry of the coils, as well as the electromagnetic coupling with the armature circuit. The electric force acting on the armature is calculated using the principle of virtual work [12], while the resulting acceleration is determined by applying Newton's second law, accounting for resistive losses and friction.

The mutual inductance between a coil and the armature is a function of their relative position. It can be calculated with high precision using numerical techniques such as finite element analysis or the filament method [11]. These methods enable accurate modeling of the cannon's behavior and support performance optimization through simulations that account for dimensional variations.

2.2. Dynamic Model of the Electromagnetic Cannon

Figure 1 presents the equivalent circuit model of the electromagnetic cannon, which consists of a charged capacitor, a thyristor, the coil, and the moving armature. The system's dynamic behavior is governed by a set of differential equations derived from Kirchhoff's voltage law, Maxwell's equations, Newton's second law, and the principle of virtual work [13]. The resulting dynamic model is expressed as [14].

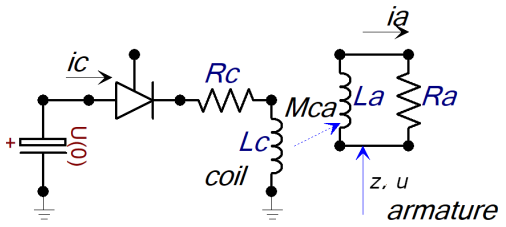

Figure 1. Equivalent circuit model of the electromagnetic cannon

$$\begin{bmatrix} v_c \\ v_a = 0 \end{bmatrix} = \begin{bmatrix} R_c & 0 \\ 0 & R_a \end{bmatrix} \begin{bmatrix} i_c \\ i_a \end{bmatrix} + \frac{d}{dt} \begin{bmatrix} \lambda_c \\ \lambda_a \end{bmatrix} \tag{1}$$

where

$$\begin{bmatrix} \lambda_c \\ \lambda_a \end{bmatrix} = \begin{bmatrix} L_c & M_{ca}(z) \\ M_{ca}(z) & L_a \end{bmatrix} \begin{bmatrix} i_c \\ i_a \end{bmatrix} \tag{2}$$

Equation (2) describes the voltage drops across the coil and the armature, incorporating both the ohmic term and the electromotive forces induced in each circuit, in accordance with Faraday's law. The mutual relationships between the flux linkages and the currents in the system are determined by applying Ampère's law and Gauss's law within the magnetic circuit.

Figure 2 provides a more detailed representation of the electromechanical system comprising the coil, the armature, and its excitation circuit. According to Newton's second law, the force acting on the armature is given by.

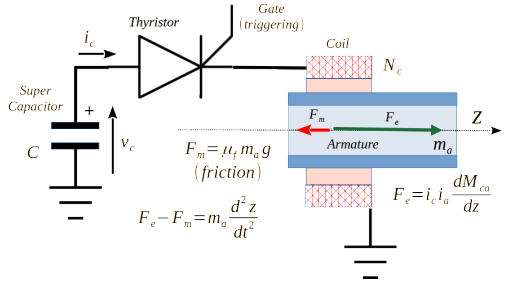

Figure 2. Electromechanical representation of the coil–armature system in the electromagnetic cannon

$$\sum F = F_e - F_m = m_a \tag{3}$$

where

$$F_e = i_c i_a \frac{\partial M_{ca}}{\partial z}; \quad F_m = \mu_f m_{ag} \tag{4}$$

and,

m_a is the mass of the armature,

μ_f is the friction coefficient,

g is the acceleration due to gravity,

The current through the coil discharges the capacitor according to the following expression:

$$C_c \frac{dv_c}{dt} = -i_c, \tag{5}$$

And due to the continuity of space, the following kinematic equation is derived:

$$\frac{dz}{dt} = u \tag{6}$$

2.3. Parameter Calculation

2.3.1. Resistance

The resistance of the coil is calculated using the following expression:

$$R_c = \rho \frac{L}{A} = \rho \frac{\pi N D}{\pi r^2} = \rho \frac{ND}{r^2}, \tag{7}$$

where $\rho = 1.68 \times 10^{-8} \Omega \cdot m$ is the resistivity of copper, N is the number of turns of the coil, D is the diameter of the circular coil, and r is the radius of the copper cross-section.

2.3.2. Friction

The dynamic friction coefficient μ_d is determined from the angle α of the inclined plane at which the moving part begins to slide [15].

$$\mu_d = \tan \alpha. \tag{8}$$

2.3.3. Dimensions of the Coil and Armature

The dimensions of the coil and armature used in this study are based on the work of Niu [7], who analyzed the timing of the shot as the armature travels through the coil. The electromagnetic cannon developed by Niu features certain dimensional variations compared to the present model. Figure 3 and Table 1 present the dimensions adopted in this work. Figure 3 illustrates a cross-sectional view at a representative azimuthal position around the z-axis, which serves as the axis of symmetry. The positions of two circular coils, each with 55 turns, are shown in red to indicate their copper composition. The solid tube representing the armature, shown in blue, moves within the coils and is assumed to be made of aluminum.

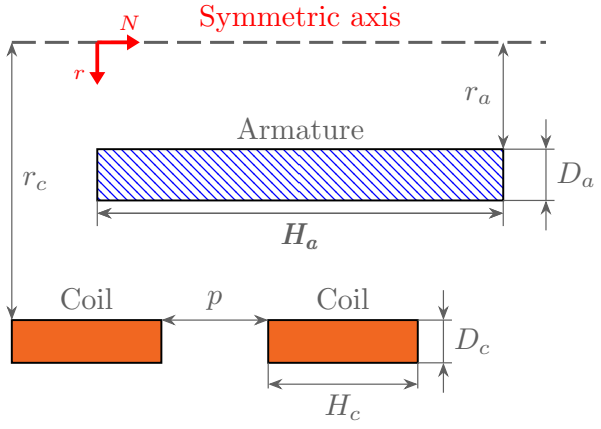

Figure 3. Geometric dimensions of the coils and armature in the electromagnetic cannon.

Table 1. Geometric and electrical parameters of the electromagnetic cannon

	Parameters	Values
Coil	r_c	10.5cm
	H_c	6cm
	p	10.5mm
	N	55
Armature	m_a	1.46kg
	r_a	8cm
	H_a	19cm
	D_a	1cm
External Excitation Circuit	C	4mF
	U_0	1.87kV
	R_c	20mΩ

2.3.4. Mutual Inductance Between the Coil and the Armature

The mutual inductances between two concentric rings separated by a distance z are calculated using the following expression:

$$M_{ij} = \frac{2\mu_0\sqrt{R_i R_j}}{k}\left[\left(1-\frac{k^2}{2}\right)K(k) - E(k)\right], \quad (9)$$

where,

$$k^2 = \frac{4R_i R_j}{(R_i+R_j)^2 + c^2}, \quad (10)$$

$K(k)$ is the complete elliptic integral of the first kind, and $E(k)$ is the complete elliptic integral of the second kind.

To determine the mutual inductance, it is necessary to compute the total magnetic flux linkage between all filaments and divide it by the current that generates this flux [11, 16].

$$M_{ac} = \frac{\lambda_{ac}}{I_{\text{coil}}} = \frac{N_{\text{coil}}N_{\text{arm}}}{n\ m\ v\ w}\sum_j\sum_i M_{ij} \quad (11)$$

The mutual inductance between the coil and the armature is calculated by accounting for the varying current densities in each filament of the armature. The equivalent inductance between the coil and the armature is then obtained using matrices of mutual and self-inductances, followed by the application of Krön reduction [17]. Consequently, the self-inductance and the mutual inductance of the armature are given by:

$$[L_{aa}] = \begin{bmatrix} L_f & M_{a1a2} & \cdots & M_{a1(v\,w)} \\ M_{a2a1} & L_f & \cdots & M_{a2(v\,w)} \\ \vdots & \vdots & \ddots & \vdots \\ M_{a(v\,w)a1} & M_{a(v\,w)a2} & \cdots & L_f \end{bmatrix} \quad (12)$$

where:

$n\,m$ is the dimension of the coil filament matrix, and

$v\,w$ is the dimension of the filament matrix representing the armature. Since all armature filaments are short-circuited, the application of Krön reduction enables the determination of the self-inductance of the equivalent circuit.

2.3.5. Self-Inductance of the Coil

The self-inductance of the coil is calculated using an expression derived from the Biot–Savart law, based on the numerical evaluation of complete elliptic integrals for a solenoidal geometry [18]. The expression is given by:

$$L_{\text{coil}} = \mu_0\left(\frac{N_{\text{coil}}}{l_{\text{coil}}}\right)^2\left\{l_{\text{coil}}^4 + \frac{4L_{\text{coil}}^2R_{\text{coil}}^2}{3D}K(k_{\text{coil}})\right\} + \ldots$$

$$\left\{\left(+4R_{\text{coil}}^2 - L_{\text{coil}}^2\right)\frac{D}{3}E(k_{\text{coil}}) - \frac{8}{3}R_{\text{coil}}^3\right\}, \quad (13)$$

where,

$$k_{\text{coil}} = \sqrt{\frac{4R_{\text{coil}}^2}{D}} \quad \text{and} \quad D = \sqrt{4R_{\text{coil}}^2 + l_{\text{coil}}^2}, \quad (14)$$

with $K(k)$ as the complete elliptic integral of the first kind and $E(k)$ as the complete elliptic integral of the second kind.

2.3.6. Self-Inductance of an Armature Filament:

The self-inductance of an individual filament is calculated using Maxwell's expression, which considers the mutual inductance between two identical circular filaments separated by the Geometric Mean Distance (GMD) [19]. The GMD is defined as:

$$\text{GMD} = e^{-\frac{1}{4}} r = 0.7788r \tag{15}$$

$$L_{ai} = \mu_0 r_i \left((1 + 0.1137\frac{R_i^2}{r_i^2}) \ln\left(\frac{8r_i}{R_i}\right)\right) + ... + \left(-0.0095\frac{R^2}{r^2} - 1.75\right) \tag{16}$$

2.3.7. VBR Model of the Cannon

The VBR model [9,14] provides an electrical and mathematical representation of the electromagnetic cannon, effectively capturing how the coil's equivalent resistance and inductance vary as the projectile traverses its trajectory. These variations are governed by the projectile's position, since the proximity of the metallic armature alters the circuit's impedance.

From (2), the flux linkage of the armature λ_a is calculated as,

$$\lambda_a = M_{ca}(z)\, i_c + L_a i_a, \tag{17}$$

obtaining i_a from (17),

$$i_a = \frac{\lambda_a - M_{ca}(z)\, i_c}{L_a}, \tag{18}$$

and substituting (18) into the armature equation (1) yields,

$$\frac{\lambda_a}{t} = -\frac{R_a}{L_a}\lambda_a + \frac{R_a}{L_a} M_{ca} i_c. \tag{19}$$

Equation (19) enables the computation of the armature flux linkage λ_a through numerical integration.

Substituting Equations (18) and (19) into the coil expression in Equation (1) results in:

$$v_c = R_{eq}\, i_c + L_{eq}\, \frac{i_c}{t} + e_e \tag{20}$$

$$R_{eq} = R_c + \frac{M_{ca}^2}{L_a^2} R_a \tag{21}$$

$$L_{eq} = L_c - \frac{M_{ca}^2}{L_a} \tag{22}$$

$$e_e = \left(v \frac{1}{L_a}\frac{dM_{ca}}{dz} - \frac{M_{ca} R_a}{L_a^2}\right)\lambda_a - 2v\frac{M_{ca}}{L_a}\frac{dM_{ca}}{dz} i_c \tag{23}$$

And from the principle of virtual work,

$$F_e = i_a\, i_c\, \frac{dM_{ca}}{dz} \tag{24}$$

Figure 4 illustrates the VBR model developed for the electromagnetic cannon, derived from expressions (21), (22), and (23). This model represents a dynamic Thèvenin equivalent that facilitates simulation within circuit analysis tools such as ATP-EMTP, Simulink, and PSIM, among other specialized platforms.

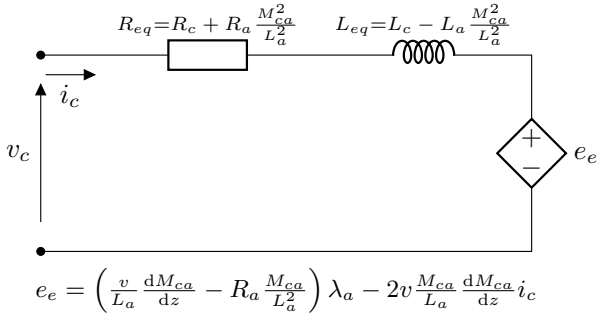

Figure 4. VBR-based equivalent circuit representing the electromagnetic interaction between the coil and the armature

2.4. Modeling in ATPDraw

The ATPDraw program is a human–machine graphical interface that facilitates the efficient use of the ATP-EMTP simulation tool. Within this environment, users can integrate complex electrical circuits, control systems (TACS), and programmable components written in the MODELS language. To simulate the behavior of the electromagnetic cannon, these three components are combined. The electrical circuit, comprising the capacitor, thyristor, and coil, is modeled using ATP-EMTP's native circuit elements. The controls for the sources and the thyristor firing are activated through TACS modules. Additionally, system dynamics and the position-dependent calculation of inductances are implemented using MODELS programming.

2.5. Equivalent Circuit of the Electromagnetic Cannon

Figure 5 shows the circuit implemented in ATPDraw to model a single stage of the electromagnetic cannon. The circuit includes a capacitor used to store the energy required for firing, a thyristor triggered via TACS, and its associated snubber circuit to mitigate transient overvoltages. Additionally, the equivalent resistance R_{eq}, inductance L_{eq}, and electromotive force E_{eq} are represented as variable components, whose instantaneous values are determined through dynamic computation using MODELS programming.

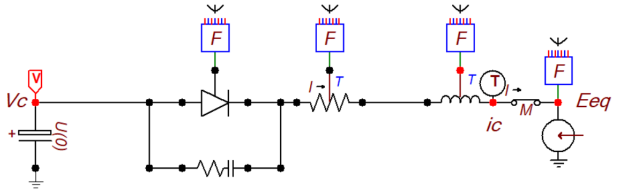

Figure 5. Equivalent circuit based on the VBR model

2.5.1. Modeling of Mutual Inductance

The mutual inductance was modeled using the filament method [11], in which the coil was discretized into $n \times m$ segments and the armature into $v \times w$ circular elements. Each segment possesses a self-inductance as defined in equation (16), while mutual inductances between segments are computed using equation (9). These expressions were implemented in a MATLAB script to evaluate the electromagnetic coupling between the coil and the armature for arbitrary relative positions along their axes. Figure 6 illustrates a representative position z at which the inductances are calculated; blue markers denote coil filaments, and red markers represent those of the armature.

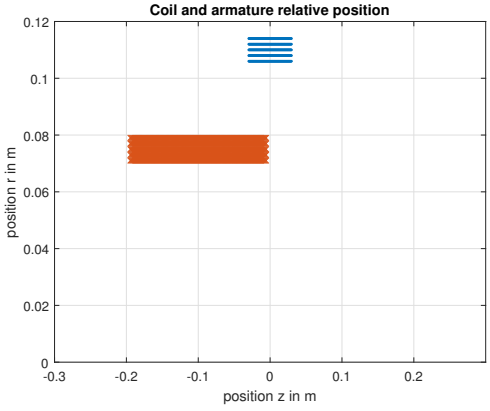

Figure 6. Representative relative position between coil and armature for mutual inductance calculation

Starting from the inductance calculations, where the electromagnetic coupling between the coil and the armature is evaluated at each separation distance between their centers, the mutual inductance as a function of position z is obtained, as illustrated in Figure 7. By applying numerical differentiation to this position-dependent mutual inductance, its spatial derivative is determined, as shown in Figure 8.

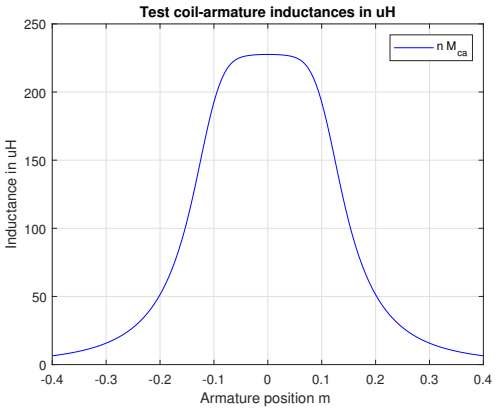

Figure 7. Mutual inductance between the coil and the armature as a function of position z, obtained from equation (11).

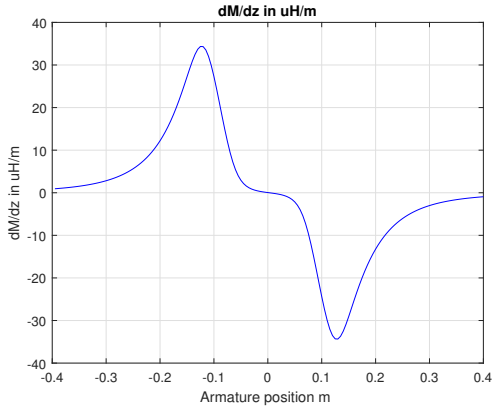

Figure 8. Spatial derivative of the mutual inductance between the coil and the armature as a function of position z

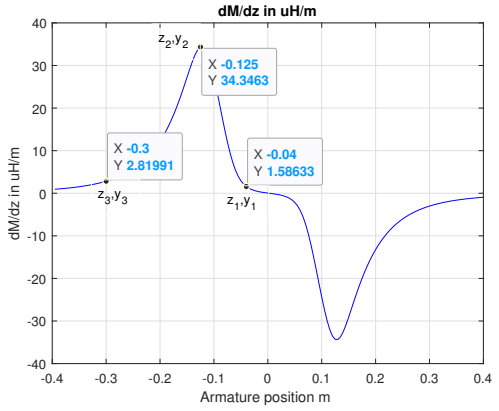

Figure 9. Extraction of key data points for graphical reconstruction

The behavior of the derivative of the mutual inductance with respect to position is subsequently reconstructed within the ATPDraw programming inter-

face. To this end, key data points are extracted from the curve in Figure 8, as illustrated in Figure 9. The derivative is modeled using three distinct functions: a horizontal line between zero and z_1, a line between z_1 and z_2, and an exponential decay between z_2 and infinity. After defining these segments based on the selected points, they are integrated to generate a continuous representation of the mutual inductance as a function of position.

2.6. Modeling of the First-Stage Coil–Armature System

The first model developed aims to replicate the interaction between a coil and the armature. To achieve this, an electrical circuit is programmed in ATPDraw, comprising a pre-charged capacitor, a thyristor with its corresponding overvoltage protection circuit, the equivalent resistance R_{eq} as defined by equation (21), the equivalent inductance L_{eq} from equation (22), and the electromotive force e_e according to equation (23).

These three quantities, R_{eq}, L_{eq}, and e_e, are dynamically computed using the MODELS module dm-m, which takes as input the armature's position, velocity, and the current in the coil. Additionally, this module calculates the electric force F_e acting on the armature. The resulting force is fed back into the MODELS module *dinamica*, which numerically integrates equations (19), (3), (5), and (6) to determine the armature's position z, velocity u, and flux linkage λ_a.

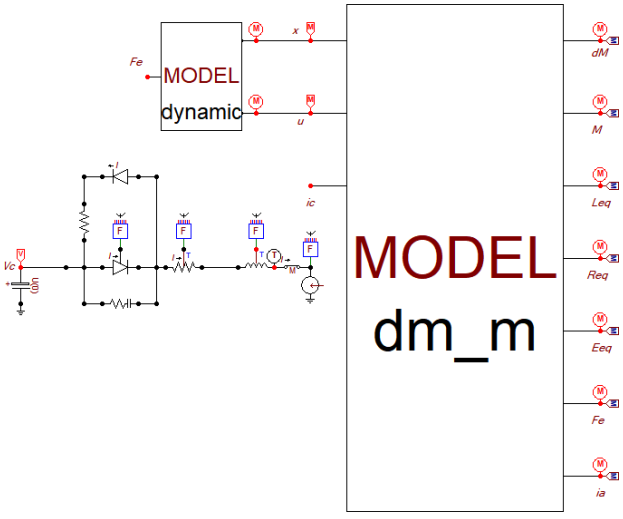

Figure 10. ATPDraw circuit used to model the first-stage coil–armature interaction

Figures 11, 12, and 13 present the simulation results for the armature velocity u, the electric force F_e acting on it, and the coil current, respectively.

Figure 11 illustrates the acceleration profile of the armature resulting from the electromagnetic force generated by current injection into the coil, as depicted in Figure 12. The electric force initially exhibits a positive peak, followed by a negative component of lower magnitude, leading the armature velocity to reach a maximum before gradually decreasing.

Figure 13 shows the behavior of the coil current. While the current follows a sinusoidal trend, characteristic of oscillations between the capacitor and the coil, it is notably influenced by the armature's motion. As the armature traverses the coil, it alters the equivalent inductance and induces an electromotive force, which delays the current's zero crossing and the subsequent deactivation of the excitation thyristor.

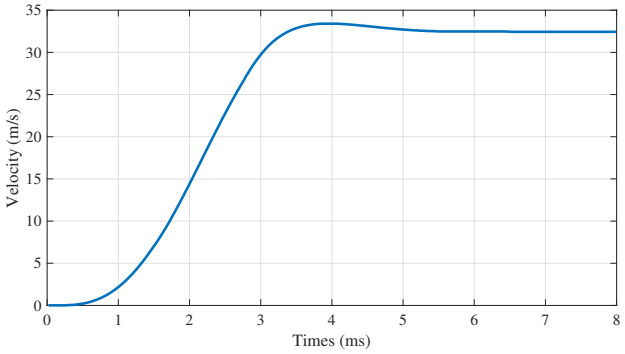

Figure 11. Velocity u of the armature for one stage cannon

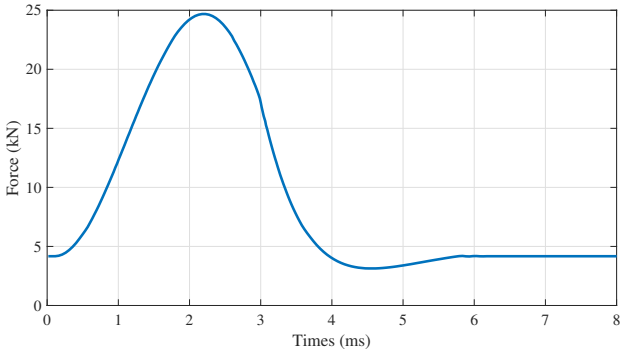

Figure 12. Electric force F_e on the armature

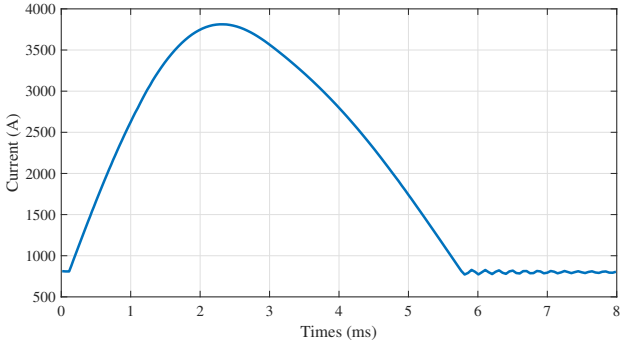

Figure 13. Current in the coil i_c

Figure 14 illustrates the reversal of current in

the armature circuit relative to the coil current, a phenomenon arising from the electromagnetic action–reaction process. Despite the reversal, the system continues to exert force on the armature, contributing to its acceleration during this interval.

Figure 15 shows the voltage behavior across the capacitor when it is connected to the coil. The system exhibits an $L-C$ type oscillation that begins at approximately 1800 V and reaches a minimum of –1500V. This voltage swing reflects both the transfer of energy to the armature and the inherent energy losses in the electrical circuit.

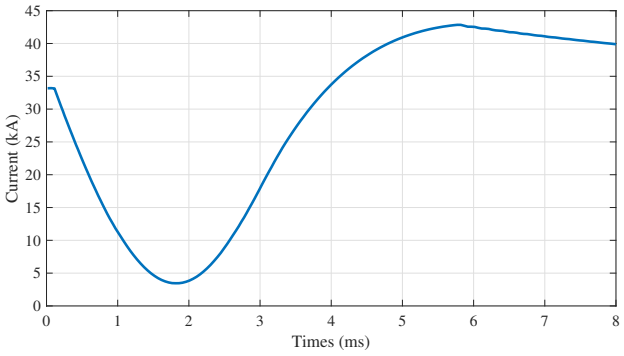

Figure 14. Armature current i_a

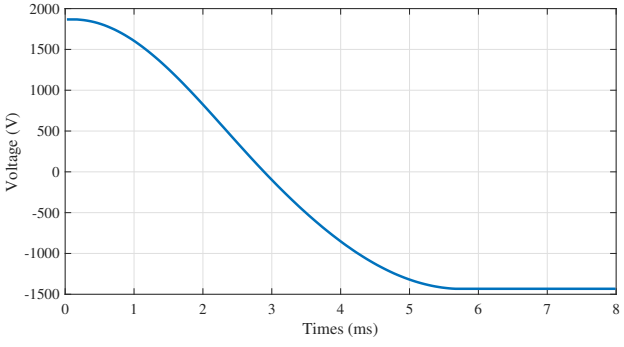

Figure 15. Voltage across the capacitor v_c during the first-stage electromagnetic cannon discharge

2.7. Cannon Model with Multiple Stages

The implementation of a multistage electromagnetic cannon involves replicating the initial single-stage model across successive stages. Each stage requires feedback of the coil current i_{ci} and the corresponding mutual inductance M_{cai}. The total electromagnetic force is computed by summing the contributions from all stages, a process carried out using a TACS module.

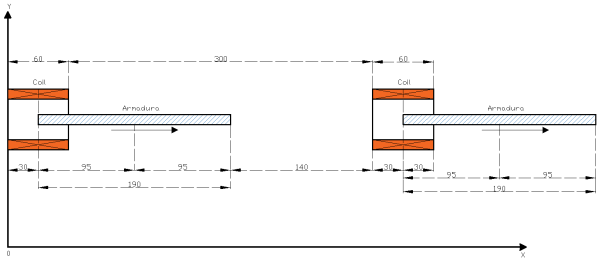

Figure 16. Definition of parameters and positions of the coils and the armature

To trigger the thyristors, it is necessary to identify the specific positions of the armature at which the activation signals are applied. The first thyristor is triggered at a predefined moment, positioning the armature optimally, typically at the midpoint of the coil when its velocity is zero. Subsequent stages are activated based on the real-time position of the armature. Improper timing of thyristor activation can negatively impact the final velocity of the projectile. A common activation criterion is to fire the thyristor when the rear end of the armature aligns with the midpoint of each coil. However, as the armature's velocity increases, advancing the firing position can enhance energy conversion efficiency. The selected trigger positions for each stage are summarized in Table 2. These values serve as reference points for coil activation and can be adjusted to optimize the system's final velocity.

Table 2. Geometric and electrical parameters of the electromagnetic cannon

Coil	Position calculation	Triggering position
1	$z+95-390$	$z-295\,mm$
2	$z+95-750$	$z-655\,mm$
3	$z+95-1110$	$z-1015\,mm$
4	$z+95-1470$	$z-1375\,mm$
5	$z+95-1830$	$z-1925\,mm$

Figure 17 presents the complete model of the electromagnetic cannon configured with five stages, constructed following the same methodology employed in the single-coil model. In this multistage configuration, an individual electrical circuit is replicated for each stage, along with corresponding MODELS modules to compute the mutual inductances and electric forces generated by each coil. Additionally, a dynamic module is employed to integrate the equations of motion and calculate the armature's flux linkage. This module receives the cumulative effect of the instantaneous forces generated by each coil of the electromagnetic cannon.

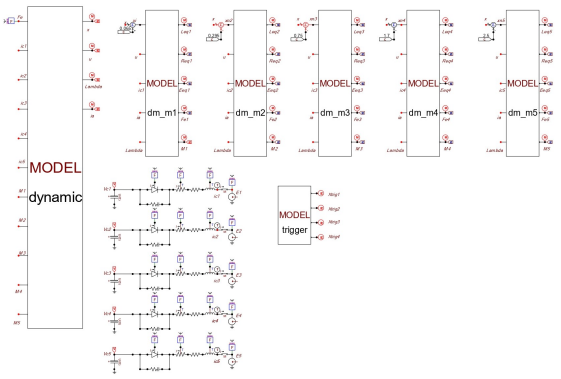

Figure 17. Five-stage Electromagnetic Cannon

Figures 18, 19, and 20 present the simulation results for the five-stage electromagnetic cannon model, depicting the armature velocity u, the electric forces F_{ei} exerted by each coil, and the corresponding coil currents i_{ci}. The velocity profile of the armature exhibits a stepped behavior, attributable to the spatial separation between the coils.

Figure 18 illustrates five distinct acceleration phases, each corresponding to the armature's passage through a coil. These accelerations result from the electromagnetic forces generated by the coils, as shown in Figure 19. Each acceleration phase resembles the behavior observed in the single-stage case (Figures 11 and 12); however, the armature's velocity progressively increases with each stage. This progression modifies the acceleration dynamics due to the varying electromotive forces induced in the coils.

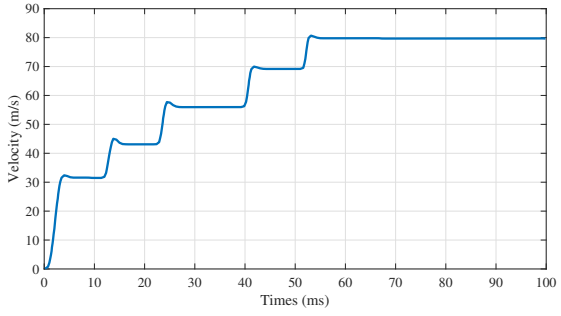

Figure 18. Velocity u during the five stages

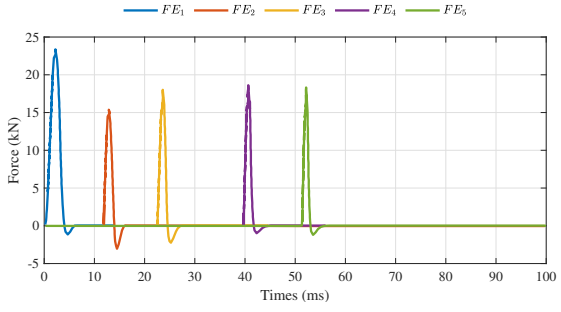

Figure 19. Electric force of the five stages

Figure 20 shows the evolution of the currents in each coil as the armature's velocity increases. At higher speeds, a noticeable change in shape occurs because the armature exits the coil entirely before the current can reach zero, thereby preventing the proper deactivation of the corresponding thyristor.

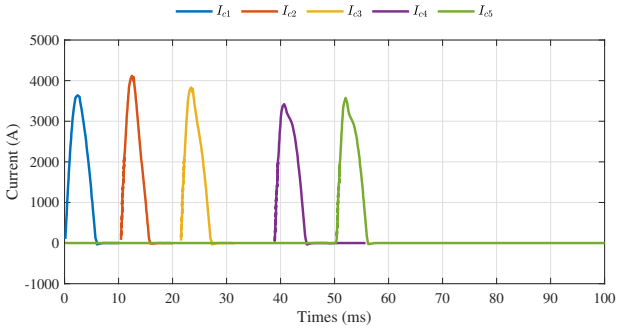

Figure 20. Current in the coil during the five stages

Figures 22 and 21 present the simulation results for the armature current and the voltages across the capacitors in each stage of the converter. The observed behavior is similar to that of a single-coil system; however, in the multistage configuration, the armature current exhibits an initial value at each triggering event. This initial current influences the generation of electromagnetic force and, consequently, the acceleration of the moving armature.

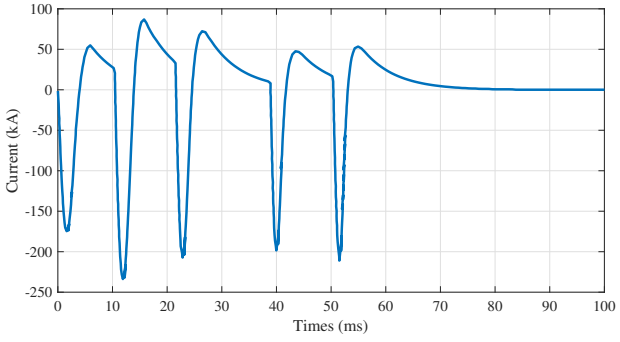

Figure 21. Armature current of the five stages.

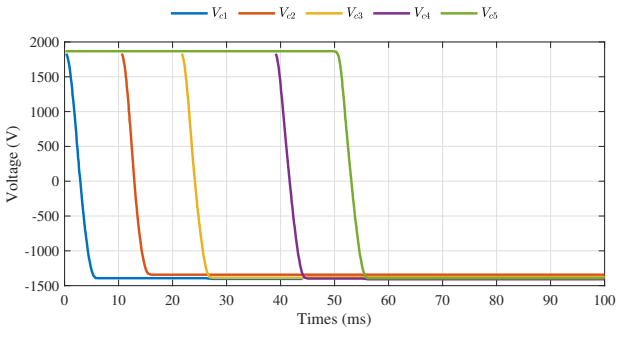

Figure 22. Capacitor voltage in the five stages

3. Results and discussion

This section summarizes the simulation results obtained using the developed model for both the single-stage and five-stage electromagnetic cannons. Additionally, the outcomes are compared with experimental data reported in the literature for a five-stage cannon [7].

3.1. Results of the First Stage

Table 3 presents the steady-state or peak values of the key variables obtained for the first-stage electromagnetic cannon model.

Table 3. Results of the first stage

Variable	Results
Velocity	$32.47\,m/s$
I_c	$3769.3\,A$
I_a	$56.8\,kA$
F_e	$24.64\,kN$

In the specific case of velocity, the steady-state value reported in Table 3 corresponds to the final value attained after the peak has been surpassed. This slight decline is attributed to the negative electric force that emerges toward the end of the coil's current pulse.

The obtained results are consistent in both form and magnitude with simulations and experiments reported in previous studies [7].

3.2. Results of the Multiple Stages

Table 4 presents the steady-state or peak values of the key variables for the five-stage electromagnetic cannon. In this configuration, the velocity increases in a stepwise manner across each stage, ultimately reaching 79.7 m/s, owing to the precise synchronization of the thyristor triggers. While this final velocity could be improved by adjusting the firing positions, such optimization lies beyond the scope of the present study. In the first stage, firing is scheduled based on time, whereas in subsequent stages it is controlled by the armature's position using a MODELS block with a triggering mechanism. The firing is slightly advanced to minimize errors and enhance energy transfer.

The relationship between velocity and force shown in Figure 19 confirms that the force peaks align with the velocity increments, underscoring the critical role of precise switching activation. A summary of the corresponding results is provided in Table 4.

Table 4. Results of each stage of the process

Stage	Variable	Result
Stage 1	Velocity	$32.47\,m/s$
	I_c	$3769.3\,A$
	I_a	$56.8\,kA$
	F_e	$24.64\,kN$
Stage 2	Velocity	$44.32\,m/s$
	I_c	$4169.23\,A$
	I_a	$88.91\,kA$
	F_e	$15.516\,kN$
Stage 3	Velocity	$58.032\,m/s$
	I_c	$3879\,A$
	I_a	$73.124\,kA$
	F_e	$18.174\,kN$
Stage 4	Velocity	$70\,m/s$
	I_c	$3467.4\,A$
	I_a	$48.189\,kA$
	F_e	$18.797\,kN$
Stage 5	Velocity	$80\,m/s$
	I_c	$3601.4\,A$
	I_a	$54.06\,kA$
	F_e	$17.9\,kN$

3.3. Comparison with Experimental Results

Experimental results for a five-stage electromagnetic cannon with dimensions similar to those used in this study are presented in [7]. The system specifically focuses on optimizing the firing synchronization of the electromagnetic cannon. The results from Niu's experiment are reproduced in Table 5.

Table 5. Results of coil current and experimental velocity

Stage	Results
Stage 1	$I_c \approx 5.66\,kA$
Stage 2	$I_c \approx 6.82\,kA$
Stage 3	$I_c \approx 7.38\,kA$
Stage 4	$I_c \approx 8.11\,kA$
Stage 5	$I_c \approx 9\,kA$
Velocity	$88\,m/s$

The comparison between Niu's model and the one developed in this work reveals that the coil currents in the proposed model are lower and exhibit a pulsating profile, whereas in Niu's model [7], the currents increase progressively. The present model reaches a final velocity of 80 m/s, slightly below the 88 m/s achieved in Niu's system. This difference may be attributed to the higher efficiency of Niu's configuration; however, both models demonstrate comparable performance in terms of energy conversion. Further improvements could be made to the proposed model and

thyristor firing system, particularly in the optimization of switching times.

3.4. Discussion

3.4.1. Evaluation of the Method Used

The modeling approach employed in this work provides a robust and reliable tool for designing electromagnetic cannons. It demonstrates strong agreement with experimental data, exhibiting discrepancies of less than 10% in critical measurable variables such as coil currents, projectile velocity, and capacitor voltages. Other parameters, including the acceleration force and armature currents, are inherently difficult to measure directly; however, they can be effectively estimated through the predictive capabilities of the proposed model.

3.4.2. Evaluation of the VBR Method

The Voltage Behind Reactance (VBR) method provides an effective framework for representing the electromagnetic behavior of the cannon through equivalent electrical circuits, transforming the coil and armature into a voltage source behind a reactance. Unlike its conventional application in induction machines, where the reactance remains constant and only the induced electromotive force varies, this implementation requires real-time adjustments to both resistance and equivalent inductance as functions of the projectile's position z. Consequently, it becomes necessary to simultaneously solve the coupled electrical and mechanical differential equations, given their strong interdependence.

3.4.3. Evaluation of the ATP-EMTP Tool

The ATP-EMTP simulation tool, along with its graphical interface ATPDraw, proved highly effective for modeling the electromagnetic cannon. These programs enable fast and efficient computation by employing the trapezoidal integration method, which models system components as networks of conductances powered by current sources at each integration step.

Given the complexity of the electromagnetic system, accurately simulating the behavior of self and mutual inductances requires the use of the filament method. To incorporate these results into the simulation, functional approximations or tabulated values are implemented within the MODELS programming environment in ATP-EMTP. In this work, precise outcomes were achieved by selecting three representative points from the derivative profile of mutual inductance between the coil and the armature. These points were then used to perform the analytical integration of these functions into MODELS programs for each coil.

The system dynamics were also successfully modeled within a MODELS module by integrating the system's state variables to compute the armature's position, velocity, and flux linkage.

3.4.4. Challenges associated with electromagnetic cannon development

The development of electromagnetic cannons presents several critical challenges that must be addressed to enable their practical deployment:

- They require high-power, compact energy sources.
- Significant energy losses, primarily converted into heat, must be efficiently managed to prevent thermal conditions that exceed the limits of structural materials.
- There are mechanical and thermal stress limits that current materials cannot exceed.
- The high projectile velocities introduce challenges for the control systems across the entire structure.
- The electromagnetic fields generated can interfere with control and communication systems, potentially disrupting their operation.
- High development and implementation costs may limit the scalability and practical adoption of these technologies.
- The reaction forces generated in the coils, comparable in magnitude to those acting on the projectile, require support systems capable of absorbing substantial mechanical stress.

4. Conclusions

This study presents the development of a computational model of an electromagnetic cannon, constructed using an analytical–numerical methodology for the calculation of self and mutual inductances in both the coils and the armature. The inductance profiles were implemented within the ATP-EMTP simulation environment using linear and exponential approximations.

The proposed model is structured into four interconnected subsystems: 1. The representation of the electrical circuit. 2. The integration of the differential equations governing the dynamic behavior of key state variables. 3. A module responsible for computing the inductances and their derivatives, as well as the electromagnetic force exerted on the armature by each coil. 4. A triggering module that activates each thyristor at appropriate armature positions. This architecture is scalable to any number of stages and emulates, with high fidelity, the principal components and dimensions of electromagnetic cannon systems.

Simulation results derived from this model exhibit deviations of less than 10% compared to experimental data reported in [7], demonstrating the approach's accuracy and robustness. Coupled with the user-friendly programming environment and visual interface offered by ATP-EMTP and ATPDraw, the proposed modeling framework constitutes a powerful tool for the analysis and design of electromagnetic launch systems. These systems hold growing relevance in diverse application areas, including military technologies, aerospace propulsion, and plasma generation for advanced scientific research.

Acknowledgments

The authors would like to express their gratitude to the Universidad Politécnica Salesiana and the Energy Research Group GIE for their invaluable support in the development and execution of this work.

Contributor Roles

- **José Manuel Aller Castro:** Conceptualization, formal analysis, investigation, methodology, supervision, writing – original draft.
- **Juan José Cordero Cantos:** Data curation, formal analysis, investigation, software, validation, visualization.
- **Pedro José León Rojas:** Data curation, formal analysis, investigation, software, validation, visualization.
- **Johnny Rengifo:** Conceptualization, methodology, visualization, writing – original draft, writing – review & editing.

References

[1] K. McKinney and P. Mongeau, "Multiple stage pulsed induction acceleration," *IEEE Transactions on Magnetics*, vol. 20, no. 2, pp. 239–242, Mar. 1984. [Online]. Available: https://doi.org/10.1109/TMAG.1984.1063089

[2] I. McNab, "Early electric gun research," *IEEE Transactions on Magnetics*, vol. 35, no. 1, pp. 250–261, 1999. [Online]. Available: https://doi.org/10.1109/20.738413

[3] E. N. Zapico, G. J. Torresán, and R. J. Garay, "Análisis estructural preliminar de un nanosatélite lanzado por cañón electromagnético," in *Mecánica Computacional*, vol. XXIV, no. 12, Córdoba, Argentina, Nov. 2005, pp. 2075–2085. [Online]. Available: https://upsalesiana.ec/ing34ar10r3

[4] J. Schroeder, J. Gully, and M. Driga, "Electromagnetic launchers for space applications," *IEEE Transactions on Magnetics*, vol. 25, no. 1, pp. 504–507, 1989. [Online]. Available: https://doi.org/10.1109/20.22590

[5] X. Niu, K. Liu, Y. Zhang, G. Xiao, and Y. Gong, "Multiobjective optimization of multistage synchronous induction coilgun based on NSGA-II," *IEEE Transactions on Plasma Science*, vol. 45, no. 7, pp. 1622–1628, Jul. 2017. [Online]. Available: https://doi.org/10.1109/TPS.2017.2706522

[6] X. Niu, W. Li, and J. Feng, "Nonparametric modeling and parameter optimization of multistage synchronous induction coilgun," *IEEE Transactions on Plasma Science*, vol. 47, no. 7, pp. 3246–3255, Jul. 2019. [Online]. Available: https://doi.org/10.1109/TPS.2019.2918157

[7] X. Niu, L. Chen, Y. An, and Y. Hu, "Research on critical trigger criterion of multistage synchronous induction coilgun," *IEEE Transactions on Plasma Science*, vol. 51, no. 9, pp. 2667–2675, Sep. 2023. [Online]. Available: https://doi.org/10.1109/TPS.2023.3306329

[8] L. Wang, J. Jatskevich, and S. D. Pekarek, "Modeling of induction machines using a voltage-behind-reactance formulation," *IEEE Transactions on Energy Conversion*, vol. 23, no. 2, pp. 382–392, Jun. 2008. [Online]. Available: https://doi.org/10.1109/TEC.2008.918601

[9] J. M. Aller, J. A. Restrepo, and J. C. Viola, "Voltage behind reactance model of induction machines using ATPDraw and MODELS," in *2021 IEEE Fifth Ecuador Technical Chapters Meeting (ETCM)*. IEEE, Oct. 2021. [Online]. Available: http://doi.org/10.1109/ETCM53643.2021.9590817

[10] H. K. Høidalen, L. Prikler, and J. Hall, "Atpdraw-graphical preprocessor to atp, windows version," in *Proceedings of International Conference on Power Systems Transients, IPST*, 1999, pp. 20–24. [Online]. Available: https://upsalesiana.ec/ing34ar10r10

[11] L. Shoubao, R. Jiangjun, P. Ying, Z. Yujiao, and Z. Yadong, "Improvement of current filament method and its application in performance analysis of induction coil gun," *IEEE Transactions on Plasma Science*, vol. 39, no. 1, pp. 382–389, Jan. 2011. [Online]. Available: http://doi.org/10.1109/TPS.2010.2047276

[12] D. C. White, *Electromagnetic energy conversion.* Wiley, 1959. [Online]. Available: https://upsalesiana.ec/ing34ar10r12

[13] J. M. Aller, "Máquinas eléctricas rotativas: Introducción a la teoría general," *Editorial Equinoccio*, 2006. [Online]. Available: https://upsalesiana.ec/ing34ar10r13

[14] J. M. Aller, J. A. Restrepo, J. C. Viola, and J. R. Mayor, "Simplified voltage behind reactance model for the six-phase open-end salient pole PMSM," in *2020 International Conference on Electrical Machines (ICEM).* IEEE, Aug. 2020, pp. 2216–2221. [Online]. Available: https://doi.org/10.1109/ICEM49940.2020.9270701

[15] Wikipedia. (2020, Apr.) Coefficient of friction. Wikipedia, the free encyclopedia. Accessed: 2025-06-12. [Online]. Available: https://upsalesiana.ec/ing34ar10r15

[16] W. G. Hurley, M. C. Duffy, J. Zhang, I. Lope, B. Kunz, and W. H. Wolfle, "A unified approach to the calculation of self- and mutual-inductance for coaxial coils in air," *IEEE Transactions on Power Electronics*, vol. 30, no. 11, pp. 6155–6162, Nov. 2015. [Online]. Available: http://doi.org/10.1109/TPEL.2015.2413493

[17] G. Kron, *A short course in tensor analysis for electrical engineers*, I. Dover Publications, Ed. CONSTABLE and CO, LTD, 1959. [Online]. Available: https://upsalesiana.ec/ing34ar10r17

[18] E. Rosa and F. Grover, *Formulas and tables for the calculation of mutual and self-inductance.* US Government Printing Office, 1912. [Online]. Available: https://upsalesiana.ec/ing34ar10r18

[19] R. Weaver, *Geometric Mean Distance - Its Derivation and Application in Inductance Calculations.* Electronbunker.ca, 06 2016. [Online]. Available: https://upsalesiana.ec/ing34ar10r19